Solution Structure of ω-Conotoxin GVIA Using 2-D NMR Spectroscopy and Relaxation Matrix Analysis†

Jonathan H. Davis,‡ Erin K. Bradley,§,‖ George P. Miljanich,⊥ Laszlo Nadasdi,⊥ J. Ramachandran,⊥ and Vladimir J. Basus*,§

Graduate Group in Biophysics and Department of Pharmaceutical Chemistry, University of California, San Francisco, California 94143-0446, and Neurex Corporation, 3760 Haven Avenue, Menlo Park, California 94025-1057

Received January 25, 1993; Revised Manuscript Received April 1, 1993

ABSTRACT: We report here the solution structure of ω-conotoxin GVIA, a peptide antagonist of the N-type neuronal voltage-sensitive calcium channel. The structure was determined using two-dimensional NMR in combination with distance geometry and restrained molecular dynamics. The full relaxation matrix analysis program MARDIGRAS was used to generate maximum and minimum distance restraints from the crosspeak intensities in NOESY spectra. The 187 restraints obtained were used in conjunction with 23 angle restraints from vicinal coupling constants as input for the structure calculations. The backbones of the best 21 structures match with an average pairwise RMSD of 0.58 Å. The structures contain a short segment of triple-stranded β-sheet involving residues 6–8, 18–21, and 24–27, making this the smallest published peptide structure to contain a triple-stranded β-sheet. Conotoxins have been shown to be effective neuroprotective agents in animal models of brain ischemia. Our results should aid in the design of novel nonpeptide compounds with potential therapeutic utility.

ω-Conotoxins are a subclass of the large family of peptide toxins found in the venom of fish-hunting sea snails of the genus *Conus* (Gray et al., 1988). Peptides from this class bind to certain subtypes of Ca^{2+} channels and thus are used to distinguish between these different subtypes (Tsien et al., 1991; Hillyard et al., 1992). ω-Conotoxin GVIA (ω-CgTx[1]), found in the venom of *Conus Geographus*, contains 27 amino acid residues and three disulfide linkages and has an amidated acyl terminus (Olivera et al., 1984). ω-CgTx binds with high affinity to neuronal N-type Ca^{2+} channels. It thus blocks the Ca^{2+} currents across the membrane of neuronal cell bodies mediated by these channels (McClesky et al., 1987) and inhibits neurotransmitter release from some presynaptic nerve terminals as well (Lipscombe et al., 1989). Administration of ω-conotoxins to rats subjected to temporary forebrain ischemia has been shown to protect neurons from subsequent neuronal degeneration (Valentino et al., 1992), presumably by inhibiting N-type Ca^{2+} channels. The three-dimensional structure of ω-CgTx reported here will aid in the design of novel nonpeptide compounds with potential therapeutic value as neuroprotective agents.

We have determined a solution structure of ω-conotoxin GVIA by two-dimensional NMR spectroscopy with the aid of distance geometry and restrained molecular dynamics calculations. The complete relaxation matrix analysis program MARDIGRAS (Borgias & James, 1989, 1990) was used to convert NOE data to distance restraints. To date, there have been published NMR structures of only α- (Pardi et al., 1989; Kobayashi et al., 1989) and μ- (Ott et al., 1991; Lancelin et al., 1991) conotoxins and no published X-ray structures of any conotoxins. A preliminary NMR study of ω-CgTx was reported by Kobayashi et al. (1988), but as it contains no assignments or detailed structural information, we initiated the independent study reported here.

MATERIALS AND METHODS

Sample Preparation. ω-Conotoxin GVIA was synthesized on a replumbed ABI Model 430A peptide synthesizer, using standard t-BOC chemistry with some modifications (Yamashiro & Li, 1988), in the manner previously described for ω-conotoxins MVIIC (Hillyard et al., 1992) and SVIA and SVIB (Ramilo et al., 1992). The synthetic preparation of ω-CgTx was subjected to amino acid analyses [described in Ramilo et al. (1992)], and the results were consistent with the expected amino acid composition (data not shown). The authenticity of our synthetic ω-CgTx was also confirmed by comparison to purified, native ω-CgTx (kindly provided by Dr. B. Olivera) and to commercially available synthetic ω-CgTx (Peninsula Laboratories, Belmont, CA) using a variety of chemical and biological methods. In particular, the chromatographic behaviors by HPLC [method described in Ramilo et al. (1992)] of all three preparations of ω-CgTx were identical (data not shown). In addition, the binding affinities of our material and the commercial ω-CgTx to rat brain synaptosomes [method described in Ramilo et al. (1992)] were the same (data not shown).

NMR Spectroscopy. Samples for NMR contained 400 μL of 10 mM protein in either 99.96% D_2O or 93% H_2O/7% D_2O at pH 4.4. All NMR spectra were collected on a GE 500-

† This research was partially supported by the National Science Foundation grant DMB9104794, National Institutes of Health grant RR01695 (I. D. Kuntz, P. I.), and a grant from REAC (U.C.S.F.) to D. A. Agard and V.J.B. J.H.D. was supported in part by NIH training grant 2 T32 GM08284.

* To whom correspondence should be addressed.
‡ Graduate Group in Biophysics, UCSF.
§ Department of Pharmaceutical Chemistry, UCSF.
‖ Present address: Chiron Corporation, Emeryville, CA 94608.
⊥ Neurex Corp.

[1] Abbreviations: ω-CgTx, ω-Conotoxin GVIA; Hyp, hydroxyproline; X, one-letter abbreviation for Hyp; NMR, nuclear magnetic resonance; COSY, correlation spectroscopy; E. COSY, edited COSY; DQF-COSY, double quantum-filtered COSY, HOHAHA, homonuclear Hartmann–Hahn; NOESY, nuclear Overhauser effect spectroscopy; DEPT, distortionless enhancement by polarization transfer; DG, distance geometry; rMD, restrained molecular dynamics; RMSD, root-mean-squared deviation. Standard abbreviations are used for amino acids.

0006-2960/93/0432-7396$04.00/0

MHz spectrometer equipped either with a GN console with a Nicolet computer or an Omega console with a Sun 3/160 computer. A DQF-COSY spectrum (Rance et al., 1983) was taken at 15 °C. HOHAHA spectra with MLEV-17 (Bax & Davis, 1985) were collected at 15 °C and 25 °C with a spin-lock time of 40 ms and at 5 °C with a spin-lock time of 70 ms. NOESY spectra (Jeener et al., 1979) were obtained at 5 and 15 °C with a 200-ms mixing time. In addition, we collected an E.COSY spectrum (Griesinger et al., 1985) at 25 °C in D_2O and one-dimensional spectra at all three temperatures.

Slowly exchanging amide protons were determined by dissolving the sample in 400 μL of D_2O and adjusting the pH to 4.4. The sample was then immediately placed in the spectrometer at the same depth as a sample of D_2O of equal volume with which we had preshimmed the magnet. A 1-D spectrum was obtained about 20 min after the exchange was initiated. A 2-D NOESY spectrum was then collected to give unambiguous assignments of the nonexchanged protons. This entire procedure was carried out at 5 °C.

In order to determine the correlation time τ_c, the ^{13}C T_1 and T_2 relaxation times were determined at natural abundance, using a sample dissolved in 99.96% D_2O. These experiments were carried out using a double-DEPT technique with proton detection for maximum sensitivity. For T_1 we used the double-DEPT with inversion-recovery (Sklenár et al., 1987), and for T_2 we used the double-DEPT sequence with a Carr–Purcell–Meiboom–Gill modification using a series of 180° pulses with a repetition rate of 1 ms to replace the single 180° refocusing pulse in the sequence of Nirmala and Wagner (1989). The data were analyzed by fitting to the proper exponential decay function.

Data Processing. Two-dimensional NMR spectra were processed on Sun Microsystems Sparc1 workstations, networked through a Sun4 server and running the UNIX operating system. The software used was originally developed in the laboratory of Dr. Kaptein at the University of Groningen, The Netherlands. Many modifications have been made by Dr. R. M. Sheek, Dr. S. Manogaran, and Mr. M. Day at USCF. For 2-D spectra, the apodization consisted of Gaussian multiplication in the t_2 dimension and $\sin^2$ multiplication with a 70° shift in the t_1 dimension, with zero filling in some cases. The typical spectrum size was 2048 complex points in the t_2 dimension and 512 complex points in t_1, zero-filled to 1024 points. Spectral widths were 6024 Hz, for a final resolution of 3 Hz in t_2 and 6 Hz in t_1. One-dimensional spectra consisted of 16K complex points. Quadrature detection in the t_1 dimension was achieved by the method of States et al. (1982) in NOESY and HOHAHA spectra and by TPPI (Marion & Wüthrich, 1983) in COSY spectra. For coupling constant determination, 1-D spectra were apodized by application of a Lorenzian-to-Gaussian transformation in order to enhance the resolution. This apodization function was applied several times until the individual peaks of each multiplet were clearly resolved, while preserving enough signal-to-noise to clearly determine the resonance positions. Peak volumes were obtained either by summing up the points within a manually selected rectangular area surrounding the crosspeak or, in case of overlap, by fitting the region to be integrated with a collection of Lorentzian lines to best represent the data, using the Sparky program[2] developed at UCSF (D. Kneller and I. D. Kuntz, manuscript in preparation).

Restraints from MARDIGRAS. Distance restraints were calculated from experimental NOESY intensities using the program MARDIGRAS (Borgias & James, 1989, 1990). MARDIGRAS uses the complete relaxation matrix to produce an upper and lower distance bound for each experimental intensity. Because it was designed to take spin-diffusion into account, MARDIGRAS eliminates the need to collect NOESY spectra at more than one mixing time. Therefore, all our data were obtained from NOESY spectra with 200-ms mixing times. Methyl groups, δ and ε pairs in the tyrosine rings, and nondistinguishable methylene pairs were treated as pseudoatoms by MARDIGRAS, with the resulting distances to the geometrical center of the proton group. For use in DG and MD calculations, these pseudoatom distances were converted into distances to the nearest heteroatom and the upper and lower bounds increased and decreased, respectively, by the distance between the pseudoatom location and the nucleus of the heteroatom. Nonstereospecifically assigned methylene protons distinguishable by chemical shift were treated individually by MARDIGRAS, but for use in calculations, a restraint to a methylene proton was converted into a restraint to the attached carbon atom, with 1 Å added to the upper bound and 1 Å subtracted from the lower bound. The exception to this conversion was when there were restraints between each of the protons of the methylene pair and another proton; in these cases the largest upper bound and smallest lower bound were used for both restraints.

Distance Restraints from Dihedral Angle Constraints. The distance geometry program used in this study cannot accept dihedral angle constraints, and many other studies do not include such constraints for DG structure calculation. We have developed a simple method of converting ϕ or χ^1 dihedral angle constraints into distance restraints usable by DG. When a bond is rotated, there is a certain set of distances between pairs of atoms that vary in a sinusoidal manner and that are fixed in the absence of bond rotation. Our method places upper and lower bounds on three of these interatomic distances to uniquely define an allowed range for a torsional angle. The three atom pairs are chosen so that for any angle constraint as large as possible a distance penalty is incurred when an angle falls outside its allowed range. The distances between all relevant atom pairs were derived by rotating the bond on an amino acid model with standard geometry. To constrain a χ^1 angle, we chose the intraresidue atom pairs Hβ2 to C, Hβ3 to C, and Hβ3 to N. By limiting these three distances to those found at the limits of the desired range around the χ^1 angle (we used ±40° from the ideal staggered conformation), the bond is allowed to rotate freely within the range, but outside the range the amount of violation of at least one distance is rapidly increasing as the violation of the angle increases. The same approach was used for the ϕ angle; in a residue n, to constrain ϕ_n we used the three interresidue distances between the O_{n-1} and C_n, Hα_n, and Cβ_n.

Structure Calculations. Distance geometry calculations were performed on the Cray Y-MP at the San Diego Supercomputer Center using the distance geometry program VEMBED (Kuntz et al., 1989), a vectorized version of EMBED (Havel et al., 1979). Restrained molecular dynamics calculations (rMD) and energy minimizations were carried out with the GROMOS-87 programs (van Gunsteren et al., 1983) using Sun Sparc2 workstations. The 37D4 force field was used, and all the calculations were performed *in vacuo* with all charged groups neutralized, using the SHAKE algorithm (van Gunsteren & Berendsen, 1987) to keep all bond lengths constant. The distance restraint constant K_{dis} was increased linearly from 0.6 to 10 kcal mol^{-1} Å^{-2} in the first 3 ps, while the temperature was kept at 600 K, followed by 2 ps at 600 K with K_{dis} = 10 kcal mol^{-1} Å^{-2}. The time

[2] For software availability, please contact I. D. Kuntz.

constant τ_{tc} for coupling to the thermal bath was set to 0.2 ps for the first 5 ps of the rMD runs and 2 ps for the next 6 ps where the temperature was allowed to drop (final temperature setting 0 K). The long time constant helps the structures to avoid getting trapped in local minima as the temperature is lowered in the annealing phase of the rMD calculations (Gippert et al., 1990). At the end of the 11-ps run, the final temperatures found were in the range of 200–300 K. These final structures were then energy minimized including a K_{dis} = 10 kcal mol^{-1} Å^{-2}. The refinement of a single structure used 2 h of CPU time on a Sparc2 workstation.

Evaluation Methods. There are many ways to evaluate the quality of an NMR structure. We evaluate the structure of ω-CgTx using some of the standard methods, such as measuring the RMSD of the matched structures[3] and listing the violations of the input distance restraints. However, the structure of a protein backbone is fully defined by its dihedral angles, and some of these angles can be evaluated both for their fit to the accepted allowed ranges and for their match to the data and to each other. The first of these criteria is measured by a Ramachandran plot (Ramachandran et al., 1963), which shows how well the ϕ/ψ angles fall into the allowed regions. To evaluate the fit of the final structures to the data, the expected $^3J_{HN\alpha}$ coupling constant is calculated from the ϕ angle of a given amino acid, and this is compared to the measured coupling constant.

The amount of variation among the structures can be measured by an order parameter S_θ (Hyberts et al., 1992) that indicates the homogeneity of a dihedral angle θ (eq 1).

$$S_\theta = \frac{1}{N}\left(\left(\sum_{j=1}^{N}\sin\theta_j\right)^2 + \left(\sum_{j=1}^{N}\cos\theta_j\right)^2\right)^{1/2} \qquad (1)$$

Here, θ_j is a particular dihedral angle θ from the jth structure out of N structures. S_θ is calculated for that particular angle only; the value of S for a single amino acid's backbone would be the average of S_ϕ and S_ψ. S_θ is functionally equivalent to the length of the vector resulting from the addition of the unit vectors representing the dihedral angles, divided by the number of vectors that were summed.

RESULTS

Identification of Spin Systems. The first step in NMR structural analysis is assignment of the NMR spectrum. We used the methods of spin-system identification and sequential linking developed by Wüthrich and co-workers (Wüthrich, 1986). In the sequence of ω-CgTx, certain residue types have chemical shift patterns in the COSY and HOHAHA spectra that allow immediate identification, while others must await sequential assignment. The most easily identified amino acids were the glycine, the hydroxyprolines, the threonines, and the four basic residues. The assignment of these residues was straightforward, with two exceptions; in one of the threonines (T23) Hα and Hβ have the same chemical shift, so there appears to be a COSY crosspeak between the methyl and the Hα. This mimics the spin system appearance of Ala; since there is no Ala in ω-CgTx, the degeneracy was immediately identified. Determining the spin system of Hyp-21 was complicated by the α and γ protons having the same chemical shift. Only after the Cδ protons were positively identified by the NOE pattern could we be sure of the assignments. The lysine and arginine residues were fully assigned, and the characteristic patterns of crosspeaks were found in the COSY and in the HOHAHA spectra.

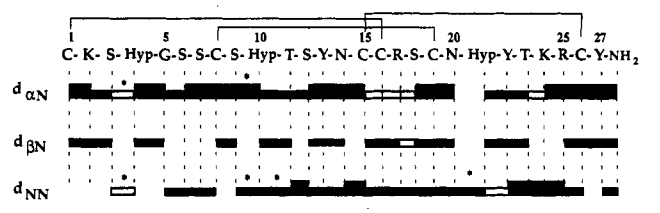

FIGURE 1: Sequential connectivities generated from NOE peaks. The intensity of the connection is indicated by the height of the box. Open squares indicate that an NOE peak was present, but the intensity could not be resolved due to overlap. Brackets above the sequence show the disulfide bonding pattern. * For Hyp residues the δ-carbon protons were used in lieu of the amide proton.

The other 17 residues all have AMX backbone spin systems (Wüthrich, 1986) and so could not be identified from only the COSY and HOHAHA spectra. From the NOESY spectrum, tyrosines were identified by the presence of crosspeaks between β and δ protons and asparagine residues identified by crosspeaks between β protons and side-chain NH_2 groups. The remaining NH_2, present in the HOHAHA and COSY, was assigned to the amidated carboxyterminus of the protein. The six serines and the six cysteines were not distinguishable until sequentially assigned.

The initial assignments were from a set of H_2O spectra at 15 °C. Water presaturation supressed the Hα resonances around 4.95 ppm, so at first we had fewer than the expected 23 amide spin systems. Spectra at 25 and 5 °C were used to find the missing peaks. Table I shows the assignments of ω-CgTx at 15 °C, with adjustments indicating the change in the chemical shift with a 10° decrease in the temperature.

Sequential Assignment. Residues are sequentially linked by NOESY crosspeaks, mostly from NH_i, $H\alpha_i$, and $H\beta_i$ to HN_{i+1}. In Hyp residues we used HCδ protons in lieu of NH. Figure 1 shows the connectivities observed in ω-CgTx. Connectivities are categorized as strong and weak, indicated by the height of the bar. In cases of severe overlap, an open bar indicates that there is a peak in the expected location, but no strength category should be inferred, since there could be other contributions to the intensity.

The sequences T11-N20 and Y22-Y27 were assigned first, as the majority of residues in those sections are of identifiable type, and so sequential assignments proceeded with great confidence. Starting with G5, the next four residues are all Ser or Cys, but there are strong $H\alpha_i - HN_{i+1}$ NOEs, so again there was no problem with the assignments. C1 was assigned as the AMX spin system that did not have an amide proton, and residues 1–3 were sequentially assigned. The C-terminal NH2 was confirmed by the presence of strong NOEs to several resonances of Y27. Finally, we identified sequential NOEs to the Hβ and HCδ protons of the Hyp residues, completing the assignment of the protein. Table I lists the complete assignments.

Calculation of τ_c. The rotational correlation time τ_c was measured using natural abundance ^{13}C-proton T_1 and T_2 measurements as described in the Experimental Section. Since these measurements were made with indirectly detected one-dimensional spectra, the only carbon whose relaxation times could be measured individually was the α-carbon of Arg-25, whose attached proton is the only one completely resolved

[3] We use two methods of evaluating the RMSD: the first is *pairwise*, where each pair of structures is matched and its RMSD calculated and then the average taken over all pairs. The second is *RMSD from the average*, where for each nucleus an average position is calculated, and then the RMS deviation from that position is calculated. The second method is used primarily when the matching takes place over a different portion of the molecule than does the RMSD measurement. In general, when examining the whole molecule with both methods, pairwise RMSD values are about 50% higher than RMSD from the average. Some authors prefer to use RMSD from the average for all evaluations, and their numbers are correspondingly lower.

Table I: ^{1}H Resonance Assignments of Conotoxin GVIA at 15 °C, pH 4.4[a]

residue	HN	Hα	Hβ2	Hβ3	others
Cys-1		4.57	3.04	3.25	
Lys-2	9.44 [+5][b]	4.65	1.87	1.94	Hγ (1.45, 1.54);[c] Hδ (1.67, 1.61); Hε 3.00
Ser-3	9.01 [+6]	4.55	(4.01)		
Hyp-4		4.22	2.13	2.45	Hγ 4.73; HOδ 6.7 [+11]; HCδ2 3.83; HCδ3 3.86
Gly-5	9.29 [+4]	(4.54, 3.66)			
Ser-6	7.72 [+1]	4.50	(3.94	3.86)	
Ser-7	8.92 [+5]	4.75	(3.91)		
Cys-8	8.40 [+1]	4.97	3.10	2.98	
Ser-9	8.41 [+10]	4.93	(4.02	3.73)	
Hyp-10		4.44	2.10	2.38	Hγ 4.58; HCδ2 3.65; HCδ3 4.04
Thr-11	7.63 [+3]	4.12	4.49		γCH$_3$ 1.15
Ser-12	7.52 [0]	4.40	(3.86)		
Tyr-13	8.13 [+2]	4.51	2.95	3.29	Hδ 7.09; Hε 6.85
Asn-14	8.28 [+3]	4.91	(3.03	2.74)	δNH$_2$ (7.58 [+5], 7.03 [+7])
Cys-15	8.74 [+5]	4.67	2.46	3.02	
Cys-16	9.51 [+3]	4.56	2.80	3.26	
Arg-17	8.40 [+3]	4.62	1.71	2.04	Hγ (1.69, 1.55); Hδ (3.18, 3.09); Hε 7.22 [+1]
Ser-18	7.22 [+1]	4.62	(4.04)		
Cys-19	8.89 [+6]	4.80	2.97	2.80	
Asn-20	7.93 [+1]	4.55	1.28	3.50	δNH$_2$ (7.49 [+6], 6.80 [+5])
			[−8]	[−2]	
Hyp-21		4.32	(2.25	1.72)	Hγ 4.32; HCδ (4.51, 3.94)
Tyr-22	8.35 [+3]	4.41	(3.16)		Hδ 7.29; Hε 6.90
Thr-23	7.10 [0]	4.25	4.25		γCH$_3$ 1.17
Lys-24	8.57 [+1]	3.64	2.07	2.37	Hγ (1.33); Hδ (1.72, 1.65); Hε 3.04; ζNH$_3$ 7.57
Arg-25	7.33 [0]	5.26	1.48	1.30	Hγ (1.64, 1.39); Hδ (3.16); Hε 7.20 [+2]
Cys-26	9.26 [+1]	4.95	2.81	3.68	
Tyr-27	9.32 [+1]	4.48	2.87	3.18	Hδ 7.31; Hε 6.87
NH$_2$					H1[d] 7.47 [+7]; H2 8.14 [+7]

[a] Chemical shifts are relative to internal TSP at 15 °C. [b] Numbers in square brackets indicate the change in chemical shift for a 10° drop in temperature, in units of 0.01 ppm. [c] Assignments in parentheses are not stereospecifically assigned. [d] Nomenclature of amidated C-terminus: H1 is cis to the carbonyl O, H2 is trans.

from all other proton resonances. Measurements were also made for the carbons whose attached protons overlapped at 4.3 ppm. The results for these two different proton chemical shifts were the same within the experimental error, with $T_1 = 0.24 \pm 0.04$ s and $T_2 = 0.16 \pm 0.03$ s. These values yield an estimate for the correlation time τ_c equal to 1.1 ± 0.5 ns, based on a pure dipole–dipole relaxation mechanism dominated by the directly attached proton. The contribution to the relaxation times for the chemical shift anisotropy mechanism can be estimated based on the parameters obtained by Norton et al. (1977) for the α-protons of proteins. These contributions were about 2 orders of magnitude longer than the observed T_1 and T_2 relaxation times, so it is a reasonable assumption to consider only the dipole–dipole mechanism.

Distance Restraints. The volume integrals obtained from the NOESY spectra were used to generate distance restraints with the aid of the program MARDIGRAS (Borgias & James, 1989, 1990). This program analyzes the complete NOE relaxation matrix to generate upper and lower bound distance restraints. Since MARDIGRAS results are quite sensitive to the estimated correlation time, we ran the program with three different input correlation times ranging from 0.6 to 1.6 ns, in order to cover the range calculated from relaxtion measurements. Each NMR restraint was given a upper and lower bound by MARDIGRAS, and we took for each final restraint the maximum upper and minimum lower bound from all runs, thus decreasing the probability that the bounds were overly tight or incorrect due to an error in the correlation time. MARDIGRAS requires a starting structural model, which it uses to supply distances where there are missing NOEs in the data. It has been shown (Thomas et al., 1991) that the distances obtained by MARDIGRAS are not very sensitive to the starting model, so for the initial set of distance restraints we used an extended chain, and the restraints produced by the program were good enough to generate a family of reasonable starting structures. These initial calculations used only those NOESY crosspeaks that had unambiguous assignments. For subsequent calculations, we used as starting structural models each of the structures obtained from the most recent refinement.

MARDIGRAS calculates each restraint individually, so there is not a uniform range to the bounds. But to give some idea of what MARDIGRAS restraints look like, we present several examples (for reference, a fixed-distance pair of β-methylenes has intensity 700): R25 NH – K24 HN, a very strong NOE with intensity 120, has distance bounds of 2.75 ± 0.25 Å; R25 HN – N20 HN, a medium-strong NOE with intensity 64, has bounds of 3.1 ± 0.3 Å; K24 HA – C8 HN, a weaker NOE with intensity 9, has bounds of 3.95 ± 0.75 Å; and R25 HA – S7 HN, a weak NOE of intensity 3.5, has bounds of 4.6 ± 0.4 Å. The complete table of restraints has been deposited in the Brookhaven Protein Data Bank, along with the coordinates of the final structures.

Stereospecific Assignments. A protein solution structure benefits greatly from the stereospecific assignment of as many methylene protons as possible (Güntert et al., 1989). β-Methylene protons can be stereospecifically assigned from a combination of the χ^1 angle coupling constant and NOE-derived distances between the β protons and the intraresidue amide proton (Wagner et al., 1987; Basus, 1989). In difficult cases, distances to neighboring residues can provide the needed information. To make initial assignments we used an extension of the method of Wagner et al. (1987) that includes the MARDIGRAS distance restraints (upper and lower bounds) and the $^3J_{HN\alpha}$ value. In this method we calculated expected Hβ to HN distances (assuming staggered geometry) for each rotamer position that was consistent with the coupling data, given the possible φ angles calculated from $^3J_{HN\alpha}$. These expected distances were compared to the upper and lower bounds generated by MARDIGRAS, and an assignment was made if a consistent and unique pattern was seen. Subse-

quently, other data such as sequential NOEs were used to confirm the χ^1 rotamers.

1-D spectra provided the $^3J_{HN\alpha}$ values (see Table II) as described in the Materials and Methods section. We measured the $^3J_{HN\alpha}$ coupling constants for 15 of the residues from the 15° spectrum. Four of the amide protons that are overlapped at 15° could be measured in the 25° or 5° spectrum, due to the differences in temperature dependence of the HN chemical shifts (see Table I). To confirm that measurements taken at different temperatures can be combined, we compared the splitting of several amides that are measurable in all three spectra, and the values agreed to within 10%. Since the $^3J_{HN\alpha}$ coupling constant is dependent on structure, the observation that these values remain essentially the same over a 20° temperature range increases our confidence that the structure remains the same and therefore that data from spectra at different temperatures within that range can be combined.

To determine the χ^1 angles, we used an E.COSY spectrum taken at 25 °C to decrease line width and maximize resolution. We measured the α/β coupling constants from the passive coupling in the crosspeaks. Stereospecific assignments and χ^1 rotamer values were determined for 13 of the 27 residues in ω-CgTx (see Table II). In addition, Hyp-4 and Hyp-10 were stereospecifically assigned on the basis of intraresidue NOE data and coupling constants. For Ser-6 and Ser-9 the α/β coupling constants were not consistent with any of the three possible rotamer conformations, indicating motional averaging. The other four serine residues and Tyr-22 have degenerate β chemical shifts, so nothing can be concluded about their orientation.

Structure Determination. The structure of ω-CgTx was determined using distance geometry (DG) to calculate initial structures and restrained molecular dynamics (rMD) to refine the structures. If a substantial number of restraints were added or changed after a rMD run, the new restraints list was given to DG, and a new set of structures was calculated and refined. New restraints were obtained by eliminating all but one possible assignment for the observed NOESY crosspeaks that had multiple assignment possibilities due to resonance overlap, based on the distances found in the previous set of calculated structures.

For the DG calculations, disulfide bonds were defined by a set of distances between each Sγ and the partner's Sγ and Hβs. We used the disulfide pairing pattern C1–C16, C8–C19, and C15–C26, as first determined for ω-CgTx by Nishiuchi et al. (1986) and confirmed specifically for the synthetic material employed in this study using a series of specific enzymatic cleavages, HPLC purification of the products, and amino acid analysis and/or amino acid sequencing (D. Chung, S. Gaur, J. Bell, L. Nadasdi, and J. Ramachandran, unpublished results). The disulfide constraints were combined with the initial MARDIGRAS distance restraints into a file which was input for DG to generate 20 starting structures. Fourteen of these 20 were kept, and the remaining six were discarded because they had the mirror image global fold. The incorrect structures were recognizable because they were in the minority and had much higher final energy values than the group of correctly folded structures. We then refined the 14 structures with rMD. Early attempts with the rMD calculations produced problems in the regions involving the disulfide linkages, so we developed a protocol of running rMD twice on each structure; for the first run we included no disulfides and used a restraint of 5 Å between the sulfur atoms of each disulfide pair. For the second run we removed that restraint and included the normal disulfide linkage in MD. The purpose was to allow MD to overcome

Table II: Dihedral Angle and Hydrogen Bond Data[a]

	1 C	K	S	X[b]	5 G	S	S	C	S	10 X	T	S	Y	N	15 C	C	R	S	C	20 N	X	Y	T	K	25 R	C	27 Y
φ angle (avg)		−73	−48	−50	105	−62	−69	−143	−94	−52	−82	−115	−39	−86	−117	−60	−115	−17	−82	−88	−55	−62	−103	57	130	66	67
order param S^c		0.98	0.92	1.0	0.99	0.99	0.99	0.98	0.98	0.99	0.95	0.92	0.52[d]	0.99	0.99	1.0	0.99	0.66	0.97	0.98	1.0	0.99	0.98	0.99	0.99	0.99	0.99
ψ angle (avg)		149	125	139	132	−34	148	128	161	144	−35	−13	47	43	39	153	−43	84	157	136	111	−41	−44	−6	31	145	135	
order param S		0.98	0.90	0.99	0.99	0.99	0.98	0.99	0.98	0.96	0.96	0.96	0.58[d]	0.99	0.99	1.0	0.99	0.68	0.99	0.99	1.0	1.0	0.99	0.99	0.99	0.99	1.0	
χ¹ angle (avg)		69	−73	30	−34		−63	−5	58	161	−25	67	17	−67	62	−62	−64	−67	−162	−169	−174	−27	−96	62	−65	−72	−60	−74
order param S		0.99	0.99	0.27	1.0		0.57	0.35	0.99	0.71	0.96	0.60	0.51	1.0	0.92	0.98	0.98	0.98	0.43	1.0	1.0	0.98	0.61	0.92	0.98	1.0	1.0	0.99
$^3J_{HN\alpha}$ coupling, Hz			6.8	4.2			5.4	4.0	8.5	7.8		8.7	7.9	6.6	8.5		4.3	9.7		7.5	6.8		7.9		7.2	9.7	2.8	5.0
χ¹ rotamer[e]			g^2g^3	t^2g^3					g^2g^3					t^2g^3		t^2g^3	t^2g^3	t^2g^3		g^2t^3	g^2t^3				t^2g^3	t^2g^3	t^2g^3	t^2g^3
slow HN exch						•															•			•	•	•	•	•
H-bond acceptor[f]			N14			S3			K24				S9	S9			K2		C15		R25			?[g]	N20	N20	S6	S18
H-bond energy[h]			−2.3			−2.1	−2.0		−2.6				−1.2	−1.7			−2.4		−1.6		−2.5				−1.5	−0.8	−2.2	−2.6
no. of structures[i]			21			21	21		21				18	8			20		9		21				21	21	21	21

[a] Structural data from the 21 best structures. [b] We use X as the one-letter abbr. for hydroxyproline. [c] Order parameter S_ψ of preceding dihedral angle (see eq 1) (Hyberts et al., 1992). [d] ψ of S12 and φ of Y13 are found in two distinct conformations with mean values for the ψ/φ pair of (−29°, 47°) and (84°, −77°). Within each conformational group the S parameter values are near 1.0. [e] Entries indicate the rotamers that were determined from coupling constant and NOE data. Nomenclature taken from Wüthrich (1986). [f] Residue containing the carbonyl oxygen that accepts the hydrogen bond from the residue in the current column. [g] Unknown H-bond acceptor, but we speculate it may be Oδ of N20, see Figure 2a. [h] Average energy in kcal of hydrogen bond, averaged among all structures where hydrogen bond was formed (hydrogen bond is formed when energy ≤−0.5 kcal). Evaluated by program DSSP (see text). [i] Number of structures in which the hydrogen bond energy was below the cutoff energy.

some of the high barriers that may have existed when the sulfur atoms were bonded to form the disulfide linkages. rMD refinement resulted in a set of structures with lower final energies and a pairwise RMSD value of the backbone atoms of 2.5 Å.

With initial structures in hand, we could then assign NOESY peaks where there were originally at least two possible assignments. In most cases the correct assignment became obvious when the possibilities were compared to the structure. We added the volume integrals for the newly assigned crosspeaks to the original peak list and then ran MARDIGRAS again to calculate a second generation list of restraints. This time instead of an extended chain for the starting structure, we had the 14 structures from the previous round, but we had no way of choosing one structure as better than another, so we ran MARDIGRAS 42 times, with 14 starting structures at each of the three τ_c values used before. For each restraint, from the 42 possibilities the highest and lowest distances were selected to become the upper and lower bounds.

For the final refinement, we added to the restraint file all usable torsional angles obtained from vicinal coupling constants, and we removed all NOE restraints that became redundant due to the coupling constant data. $^3J_{HN\alpha}$ coupling constants were converted to ϕ angle constraints according to the following rules: if $^3J_{HN\alpha} \leq 5.5$ Hz, then we constrained ϕ to the range $-90° < \phi < -40°$, and if 10.0 Hz $\geq {}^3J_{HN\alpha} \geq$ 8.5 Hz, then the range was $-160° < \phi < -80°$ (Pardi et al, 1984). Five residues with $^3J_{HN\alpha} \leq 5.5$ Hz and three with $^3J_{HN\alpha} \geq 8.5$ Hz were constrained by these rules. (Three other residues that fell into one or the other of these categories were not constrained, but their ϕ angles after refinement agreed with their $^3J_{HN\alpha}$, as shown in Figure 6). The 13 χ^1 angles whose orientations had been determined were constrained such that there was no penalty for deviation of ±40° from the ideal rotamer position ($\chi^1 = +60°, -60°$, or $+180°$). Furthermore, we included the stereospecific assignments, and with these new constraints we generated 38 DG structures, of which the best 21 were chosen. These were refined with rMD as before, and the pairwise RMSD of the backbone atoms was 0.93 Å. The number of substantial distance violations was reduced from the earlier structures, but there were still some restraints that were violated in most of all structures by >0.5 Å. We carefully examined all restraints that were violated in many structures and found two that were determined to be noise and two others whose assignments were still ambiguous. These four restraints were removed from the file. There were two restraints whose upper bounds were violated in all structures and whose MARDIGRAS maximum distances were around 4.0 Å. These peaks were small in a NOESY with a 200-ms mixing time, and since it is common procedure to give a maximum distance of 5.5 Å for such crosspeaks, we loosened these restraints accordingly.

The already refined structures were then refined once more with the final restraints file, using a single run of rMD (including disulfides). This set of structures had an average pairwise backbone RMSD of 0.58 Å, and the RMSD for all heavy atoms was 1.46 Å. The number of violations was low, and there were no upper bound violations of over 0.5 Å in the entire set of structures (see Table III). At this point we felt the structural refinement was complete.

Table III: Restraint Violations[a]

violation range	av no. of upper bound violations[b]	av no. of lower bound violations[c]
violation > 0.5 Å	0	0.10
0.5 Å ≥ violation > 0.4 Å	0.24	0.10
0.4 Å ≥ violation > 0.3 Å	0.71	0.29
0.3 Å ≥ violation > 0.2 Å	1.9	1.3
0.2 Å ≥ violation > 0.1 Å	7.0	5.8

[a] Violations of the restraints used in the structure calculations of the best 21 structures. [b] Average number of violations per structure for the ranges given. [c] MARDIGRAS provides lower bounds for each restraint. Violations occur when the distance is less than this lower bound.

DISCUSSION AND EVALUATION OF STRUCTURE

Hydrogen Bonds. The hydrogen-exchange experiment identified seven slowly exchanging protons in the structure, and these were examined to find likely bonding partners. The final structures were also examined for potential hydrogen bonds whose donors were not found to be slowly exchanging. We used the program DSSP (Kabsch & Sander, 1983) to determine hydrogen bonding partners. DSSP evaluates the energy of the bond, so there is not a specific distance or angle cutoff, but instead an energy cutoff. In addition, the energy value gives a good indication of the strength of the bond. Kabsch and Sander have scaled the calculations such that ideal hydrogen bond geometry results in an energy of −3.0 kcal/mol. They also suggest a maximum energy cutoff of −0.5 kcal/mol, above which a hydrogen bond does not exist. We used these criteria to identify eight unambiguous hydrogen bonds that were formed in at least 20 of the 21 refined structures and that had average energies of <−2.0 kcal/mol. Four of these hydrogen bonds involved slowly exchanging amides. Two more slowly exchanging amides, K24 and R25, form hydrogen bonds to the carbonyl of N20 in all structures, indicating a bifurcated hydrogen bond. The energy of these bonds is higher than −2.0 kcal/mol, which is not unexpected in a bifurcated bond. Several other potential hydrogen bonds were found in nine or more structures. S12 (HN) to S9 (O) stabilizes the turn at that location and is formed in 18 structures. A hydrogen bond between S18 (HN) and C15 (O) is present in only nine structures, and the structural implications of this feature are discussed below.

The other slowly exchanging amide proton belongs to T23, and it does not have an unambiguous acceptor. One possibility is that it is hydrogen bonded to the δ carbonyl oxygen of N20, which is oriented approximately correctly. However, the average distance is 3.28 Å, which does not indicate a strong hydrogen bond. The proposed hydrogen bond network for the central portion of the molecule is shown in Figure 2a, and the pairings and energies are summarized in Table II.

Structural Features. ω-CgTx has an antiparallel triple-stranded β-sheet of classification +2x, −1 (Richardson, 1981) as shown in Figure 2b. The β-sheet is its best-defined region, though the molecule has a well-defined backbone over its entire length, as can be seen from the overlay of structures in Figure 3. The largest portion of the β-sheet is from S18 to the C-terminal Y27, connected by a hairpin turn from Hyp-21 to K24. A third, short piece of β strand between S6 and C8 is hydrogen bonded to K24 through C26, making ω-CgTx the smallest known protein with a triple-stranded β-sheet. When the structures are matched to the backbones of residues 18–27, the backbone RMSD (from the average) of the residues in the sheet is 0.28 Å (see Figure 4a).

We examined the structure to identify turns, using the definition that a turn exists where two Cα's are separated by two residues and less than 7 Å (Lewis et al., 1973). Candidates were then classified according to published definitions (Richardson, 1981; Wilmot & Thornton, 1990). There is a hairpin turn between Hyp-21 and Lys-24, with ϕ/ψ dihedral pattern $\alpha_R\alpha_R\gamma_R\alpha_L$. Sibanda et al. (1989) classify this pattern as a 4:4 turn. Position 4 is a Lys, not the preferred Gly, but its

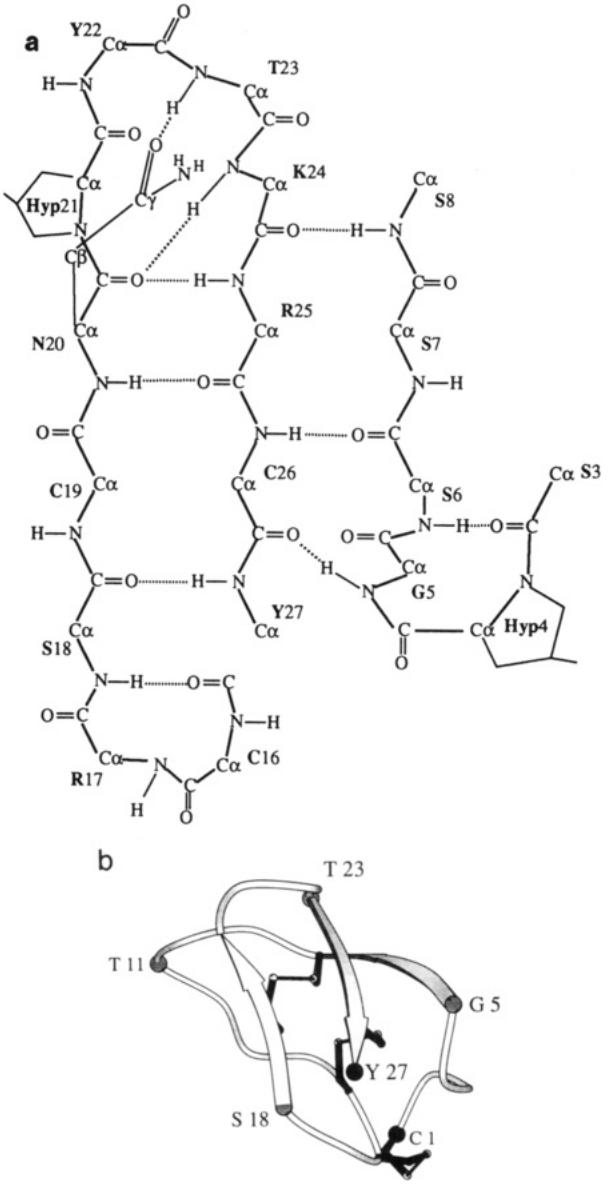

FIGURE 2: Diagrams of the structure of ω-CgTx. (a) A depiction of the consensus hydrogen bond network. Only the central portion of the molecule is shown. Note that the HN of S18 is shown rotated in, making the hydrogen bond with C15. In some of the structures, the HN of S18 is rotated away from the turn (see Figure 4c). Although only speculated, the hydrogen bond between HN of T23 and Oδ1 of N20 is also indicated. (b) Jane Richardson (1981) diagram of the secondary structure of ω-CgTx. The backbone is shown as either coil or β-sheet, and disulfide bonds are represented by small balls and dark sticks. Labeled large balls are α-carbons to serve as signposts; the terminal residues are black.

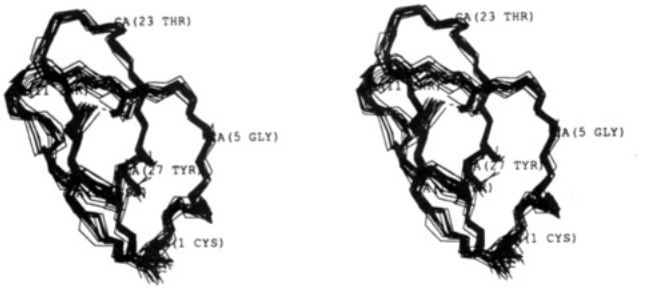

FIGURE 3: Stereoview of the backbone of the best 21 structures of ω-CgTx, superimposed so as to minimize the pairwise RMSD. Cys side chains are shown and disulfides indicated by dashed lines.

ϕ/ψ is in the small α_L region that mimics the conformation that would be found in a fourth position Gly. S3 to S6 form a type II turn in all structures, held together by a hydrogen bond between those two residues. The glycine in position 3 of the turn is common for a type II turn, and this Gly (G5) is conserved in all known ω-conotoxins (Hillyard et al., 1989; Gray et al., 1988), leading to the possibility that the turn also is conserved among ω-conotoxins.

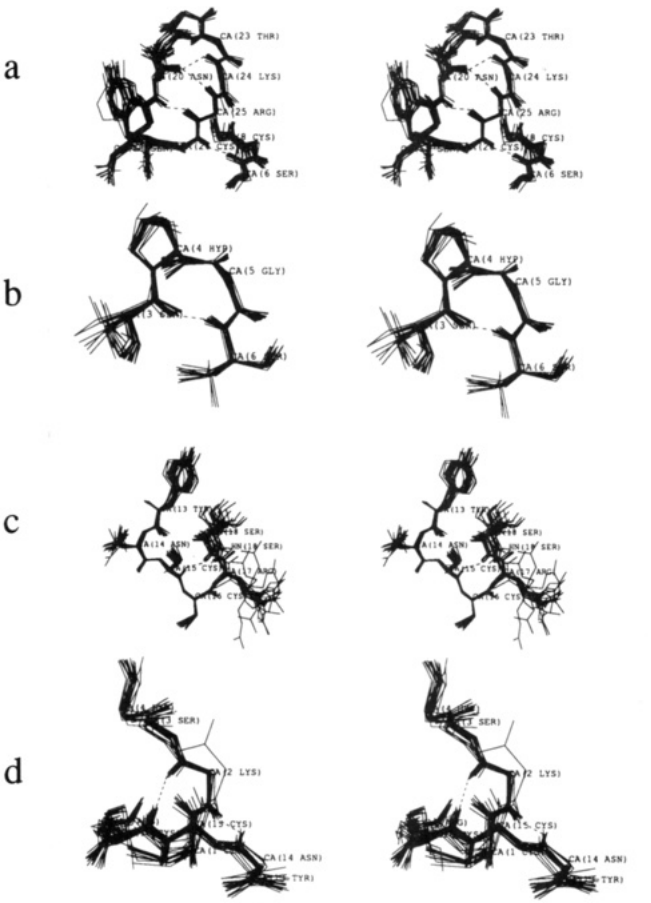

FIGURE 4: Various portions of the molecule; in each case the matching was only over the portion of the backbone pictured. However, RMSDs reported here are the backbone RMSDs from the average from globally matched structures, averaged over all residues shown in fragment. Proposed hydrogen bonds are indicate by a dashed line. (A) β-sheet portion: S18–Y27 and S6–C8; RMSD is 0.34 Å. (B) Type-II turn: S3–S6; RMSD is 0.31. (C) Type-I or -VIII turn: C15–S18; RMSD is 0.35. (D) Hydrogen bond network at N-terminal stretch: RMSD is 0.38.

Two turns were found in the stretch from S9 to S18; S9 to S12 forms a type-I turn, with the hydrogen bond between 9 and 12 formed in 17 of the 21 structures (see Figure 4b). Between C15 and S18 there is a turn, but its classification varies among the structures, due to the broad distribution of the ϕ angles of S18. In nine of the structures a hydrogen bond is formed between HN of S18 and O of C15, and the turn is a type I. However, in the remaining structures, the ϕ angle of S18 is positive and the HN is rotated out of hydrogen bonding distance (see Figure 4c). In these conformations the turn is classified as the somewhat unusual type VIII, as recently defined by Wilmot and Thornton (1990). We are presently unable to determine whether this ambiguity is due to multiple conformations or to a lack of restraints on the backbone.

Both termini are well defined in all structures. This is not surprising, given the presence of disulfide bonds constraining the ends. Figure 4d shows the hydrogen bonding pattern between the N-terminal portion and the stretch between N14 and C16, where there are two hydrogen bonds in the absence of recognizable secondary structure. The δ hydroxyl proton of Hyp-4 is exchanging slowly enough to be seen in the 5° and 15° HOHAHA and NOESY spectra and has NOEs to several

protons on Y27 and the C-terminal NH_2. The slow exchange implies a hydrogen bond, and the likely acceptor is the carbonyl oxygen of Y27. However, this hydrogen bond is not formed in the structures reported in this paper, as the average distance between Hδ1 of Hyp-4 and O of Y27 is 3.67 Å. The loop between Cys-8 and Asn-14 is the generally least well-defined region, but it is still well ordered, with a backbone RMSD from the average of 0.55 Å, when calculated from structures that were matched over the entire backbone.

Examination of the orientation of the side chains, by looking at the $^3J_{\alpha\beta}$ coupling constants, showed that all the longer side chains have well-defined χ^1 angles, with the exception of Y22, which is on the outside of a turn. This implies that the locations of the positively-charged groups and two of the tyrosine hydroxyls are at least somewhat constrained, which may have implications for the function of the molecule. One particular feature is Tyr-27, which is oriented so that the ring extends back up over the β-sheet. Hβ2 of N20 is shifted about 2 ppm upfield from its expected chemical shift, and it appears to sit under the ring of Y27. All the serines could be rotating freely, either from the evidence of their averaging coupling constants or from the fact that their Hβ chemical shifts are degenerate. Table II shows the average χ^1 angles for all the residues, and the order parameter S (eq 1) indicates the homogeneity of the angle among the 21 final structures.

Evaluation of Structure. Kobayashi et al. (1988) have reported preliminary NMR structural studies on ω-CgTx. Their report contains no NOE, structural, or assignment data that we can use to compare their structure to ours. There is a ribbon diagram (not in stereo) that gives an indication of the topology of their structure. We have carefully examined the diagram, and it appears that the β-sheet is not formed, and several other prominent features are missing (e.g., the loop from S3 to S6). However, in the absence of more data it is impossible to quantitatively discuss their work in relation to ours. Since to our knowledge this is their only publication concerning ω-CgTx, we will make no further comparisons to their work.

Evaluation in the manner outlined in Materials and Methods (*vide supra*) indicates that the structure for ω-CgTx reported here is substantially correct. The average pairwise RMSD of the backbone of the whole molecule among the 21 best structures is 0.58 Å, and the RMSD including all the heavy atoms is 1.46 Å. An examination of the RMSD from the average of each individual residue, when the backbones are matched globally, shows no stretch with particularly high RMSD (see Figure 5). The loop between S9 and N14 is the most disordered stretch of backbone, and the side chain of Tyr-22 is not constrained. The violations of NOE restraints are shown in Table III. The paucity of large violations indicates a good fit between the data and the structures. The average violation of one upper bound restraint is >0.2 Å, and all others are <0.12 Å.

There is a close correlation between the observed $^3J_{HN\alpha}$ coupling constants and the expected values based on the φ angles found in the structures, as shown in Figure 6. Of the 19 coupling constants measured, only eight were used to generate restraints for structural determination (shown as open triangles or squares). These eight are at the extreme limits, where a single range of φ angles can be confidently predicted. Thus, the fact that the remaining 11 measured values also correspond reasonably well to the φ angles of the refined structures improves our confidence in the reliability of the structures. In addition, two coupling constant values at the upper extreme (≥8.5 Hz) and one in the lower range (≤5.5 Hz) (open circles in Figure 6), which should have been converted to angle constraints, were inadvertently omitted from the restraints file, yet their φ angles in the structures agree with those predicted from the measured coupling constants. The data for Y13 have been split into two points (solid triangles) in Figure 6 because that Φ angle (and the ψ of S12) has two distinct conformers (eight with positive Φ and 13 with negative). Instead of calculating a fairly meaningless mean and standard deviation for the entire set of 21 structures, we have treated the two conformers separately, and the data

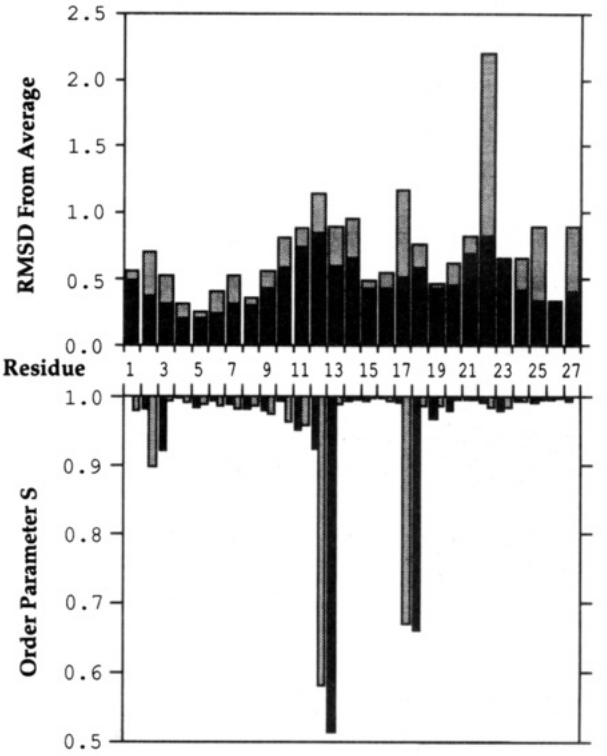

FIGURE 5: Backbone variability by residue. Top: RMS deviation. The solid bars rising from the horizontal indicate the RMSD of the backbone atoms for each residue, and the shaded bars indicate the RMSD of all heavy atoms. All RMSDs are from the average of globally-matched structures. The shaded bars include the length of the solid bars underneath. Bottom: Order parameter *S*. The descending bars show the order parameters *S* of the φ (solid bars) and ψ (shaded bars) angles, 0 = randomly distributed, and 1 = perfectly aligned (see eq 1).

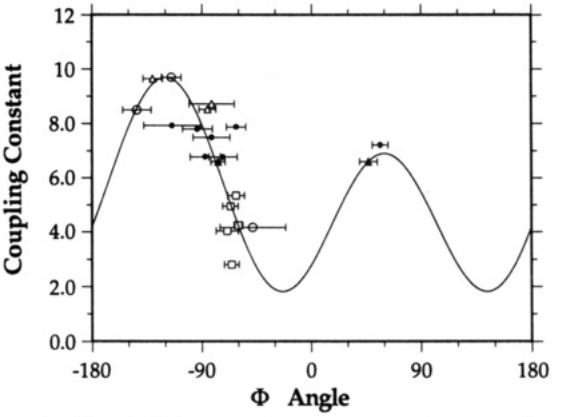

FIGURE 6: Plot of $^3J_{HN\alpha}$ coupling constant vs φ angle. Line is calculated from the equation proposed by Wüthrich (1986): $^3J_{HN\alpha} = 6.4\cos^2\phi^* - 1.4\cos\phi^* + 1.9$, where $\phi^* = \phi - 60°$. Data points indicate the mean values of the φ angles among the 21 structures, for all 19 residues for which coupling constants were measured and unambiguous. The error bars show one σ from the mean φ angle value. Open triangles represent torsional angles that were constrained to $-160° \le \phi \le -80°$. Open squares represent torsional angles that were constrained to $-90° \le \phi \le -40°$ (see Materials and Methods). Open circles were not constrained in rMD (see text). Solid triangles are the two conformations of Y13, treated independently.

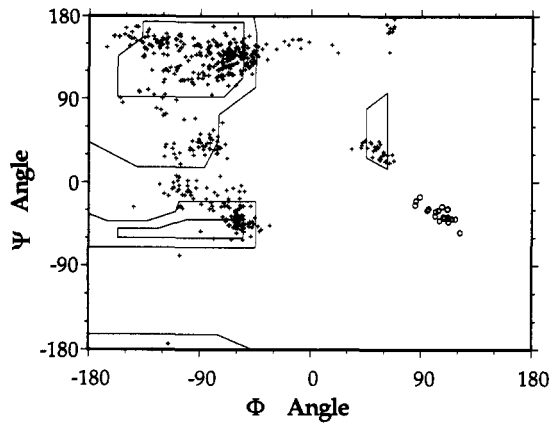

FIGURE 7: Ramachandran plot of $\phi - \psi$ angles for the best 21 structures of ω-CgTx. Open circles are Gly-5.

points reflect this division. Both conformers are consistent with $^3J_{HN\alpha}$ data.

A comparison of the order parameter S with the RMSD data (see Figure 5) highlights an interesting observation that reflects upon the meaning of some of the numbers that NMR spectroscopists use to evaluate their structures. In this figure, the single-residue backbone RMSD is calculated as an RMSD from an average structure, when all structures have been globally superimposed. There are two main regions of backbone disorder: residues centering around Ser-12 and those around Tyr-22. Yet the S parameter plot shows that while the high RMSD values around S12 are matched by low S parameters (high disorder), the S parameters around Y22 are close to 1.0, indicating a well-ordered turn. The source of the high RMSD for Y22 is in the placement of the turn within the structure; Y22 is at the outside of a hairpin at the end of a sheet, where small variations in angles closer to the center of the molecule are amplified. While this kind of amplification of small variations can be avoided by matching only a small portion of the molecule, a decision must be made on which residues to match, and this decision affects the RMSD values. In contrast, the S parameter provides a measure that is completely independent of how the structures match and is therefore an objective measure of disorder. Furthermore, the S parameter indicates the source of disorder; in the region around R17–S18 there is very high disorder of one carbonyl, resulting in a low S value for the adjoining ψ/ϕ pair. Yet the slight increase in RMSD for this region does not distinguish between minor disorder over many atoms and large variations in only a few atoms.

The final evaluating criterion is the Ramachandran plot (Ramachandran et al., 1963). For the 21 structures reported here, it indicates good overall placement of backbone dihedral angles within the allowed regions of the plot (see Figure 7). Almost all of the points in the disallowed region in the top center area are from S18, which has a poorly-defined ϕ angle. All other residues are generally within the allowed regions.

Comparison to Other Toxins. ω-CgTx is smaller than most other known peptide neurotoxins, the exceptions being other conotoxins. The only conotoxins with previously published structures are μ-conotoxin GIIIA (Ott et al., 1991; Lancelin et al., 1991) and α-conotoxin G1 (Pardi et al., 1989; Kobayashi et al., 1989). Both of these peptides are smaller than ω-CgTx and have a substantially-different disulfide topology, and neither has a triple-stranded β-sheet. Therefore, we will not compare them further to ω-CgTx. However, the basic topology of the triple-stranded β-sheet in ω-CgTx can be compared to the similar domain found in other toxin molecules.

The β-sheet topology of +2x, −1 (Richardson, 1981) is common among many smaller toxins, including the scorpion toxin AaH IT (Darbon et al., 1991) and the C-terminal portion of the sheet of Sh I from the sea anemone *Stichodactyla helianthus* (Fogh et al., 1990). This pattern has also been noticed in defensins such as HNP-3 (Hill et al., 1991), although the defensins are dimers and have a method of action completely different from that of neurotoxins. It is interesting to note that snake neurotoxins such as cobratoxin (Betzel et al., 1991), erabutoxin (Smith et al., 1988), and α-neurotoxin from Black Mamba (Brown & Wüthrich, 1992) have a reversed pattern in their triple-stranded β-sheet of −1, +2x.

Conclusion. We have presented the solution structure for the ω-conotoxin GVIA based on NMR spectroscopic data. The structure contains a triple-stranded β-sheet and four tight turns and is well-defined over its entire length. It differs significantly from the previously published structures of α- and μ-conotoxins. Such divergence is not unexpected, for while all are found in the venom of similar organisms, the ω-conotoxins bind to voltage-activated calcium channels, while the α-conotoxins bind to the nicotinic acetylcholine receptors, and the μ-conotoxins bind to voltage-activated sodium channels.

The coordinates for the final 21 structures and the input restraints will be deposited in the Protein Data Bank, Brookhaven National Laboratory, Upton, NY 11973, from where these results can be obtained.

NOTE ADDED IN PROOF

While this manuscript was being reviewed, a communication was published [Sevilla, P., Bruix, M., Santoro, J., Gago, F., Garcia, A. G., & Rico, M. (1993) *Biochem. Biophys. Res. Commun. 192*, 1238–1244] with a preliminary structure of ω-CgTx, submitted about two months later than our manuscript. Their structure appears similar to ours, but the average pairwise backbone atom RMSD for their eight final structures was 1.18 Å, while our 21 final structures had an average pairwise backbone atom RMSD of 0.58 Å. In addition, there are some discrepancies in assignments.

ACKNOWLEDGMENT

We thank Mr. Mark Day for the use of his NMR data analysis programs and Dr. Eric Fauman and Ms. Julie Newdoll for help with the figures. Part of the work was performed in the laboratory of Dr. David A. Agard. Graphical representation of our results was done in the UCSF Computer Graphics Laboratory (NIH RR-1081, Dr. R. Langridge, P.I.). The Richardson diagram was created by the program Molscript, and we thank its author, Per Kraulis. We gratefully acknowledge the San Diego Supercomputer Center for the use of their Cray-YMP. Special thanks go to Dr. Bernard D. Davis for expert editorial advice and to Dr. David Baker for helpful discussions.

REFERENCES

Basus, V. J. (1989) in *Methods in Enzymology* (Oppenheimer, N. J., & James, T. L., Eds.) *177*, pp 132–49, Academic Press, Orlando, FL.

Bax, A., & Davis, D. G. (1985) *J. Magn. Reson. 65*, 355–359.

Betzel, C., Gange, G., Pal, G. P., Wilson, K. S., Maelicke, A., & Saenger, W. (1991) *J. Biol. Chem. 266*, 21530–21536.

Borgias, B. A., & James, T. L. (1989) *Methods Enzymol. 176*, 168–183.

Borgias, B. A., & James, T. L. (1990) *J. Magn. Reson. 87*, 475–487.

Brown, L. R., & Wüthrich, K. (1992) *J. Mol. Biol. 227*, 1118–1135.

Darbon, H., Weber, C., & Braun, W. (1991) *Biochemistry 30*, 1836–1845.

Fogh, R. H., Kem, W. R., & Norton, R. S. (1990) *J. Biol. Chem. 265*, 13016–13028.
Gippert, G. P., Ping, F. Y., Wright, P. E., & Case, D. A. (1990) *Biochem. Pharmacol. 40*, 15–22.
Gray, W. R., Olivera, B. M., & Cruz, L. J. (1988) *Ann. Rev. Biochem. 57*, 665–700.
Griesinger, C., Sørensen, O. W., & Ernst, R. R. (1985) *J. Am. Chem. Soc. 107*, 6394.
Güntert, P., Braun, W., Billeter, M., & Wüthrich, K. (1989) *J. Am. Chem. Soc. 111*, 3997–4004.
Havel, T. F., Crippen, G. M., & Kuntz, I. D. (1979) *Biopolymers 18*, 73–81.
Hill, C. P., Yee, J., Selsted, M. E., & Eisenberg, D. (1991) *Science 251*, 1481–1485.
Hillyard, D. R., Monje, V. D., Mintz, I. M., Bean, B. P., Nadasdi, L., Ramachandran, J., Miljanich, G., Azimi-Zoonooz, A., McIntosh, J. M., Cruz, L. J., Imperial, J. S., & Olivera, B. M. (1992) *Neuron 9*, 69–77.
Hillyard, D. R., Olivera, B. M., Woodward, S., Corpuz, G. P., Gray, W. R., Ramilo, C. A., & Cruz, L. J. (1989) *Biochemistry 28*, 358–61.
Hyberts, S. G., Goldberg, M. S., Havel, T. F., & Wagner, G. (1992) *Protein Sci. 1*, 736–751.
Jeener, J., Meier, B. H., Bachmann, P., & Ernst, R. R. (1979) *J. Chem. Phys. 71*, 4546–53.
Kabsch, W., & Sander, C. (1983) *Biopolymers 22*, 2577–2637.
Kobayashi, Y., Ohkubo, T., Nishimura, S., Kyogoku, Y., Shimada, K., Minobe, M., Nishiuchi, Y., Sakakibara, S., & Gō, N. (1988) *Peptide Chemistry 1987*, 85–88.
Kobayashi, Y., Ohkubo, T., Kyogoku, Y., Nishiuchi, Y., Sakakibara, S., Braun, W., & Gō, N. (1989) *Biochemistry 28*, 4853–60.
Kuntz, I. D., Thomason, J. F., and Oshiro, C. M. (1989) in *Methods in Enzymology* (Oppenheimer, N. J., & James, T. L., Eds.) *177*, pp 159–204, Academic Press, Orlando, FL.
Lancelin, J-M., Khoda, D., Tate, S., Yanagawa, Y., Abe, T., Satake, M., & Inagaki, F. (1991) *Biochemistry 30*, 6908–16.
Lewis, P. N., Momany, F. A., & Scheraga, H. A. (1973) *Biochim. Biophys. Acta 303*, 211–229.
Lipscombe, D., Kongsamut, S., & Tsien, R. W. (1989) *Nature 340*, 639–642.
Marion, D., & Wüthrich, K. (1983) *Biochem. Biophys. Res. Commun. 113*, 967.
McLeskey, E. W., Fox, A. P., Feldman, D. H., Cruz, L. J., Olivera, B. M., Tsien, R. W., & Yoshikami, D. (1987) *Proc. Natl. Sci. U.S.A. 84*, 4327–4331.
Nirmala, N. R., & Wagner, G. (1989) *J. Magn. Reson. 82*, 659–61.
Nishiuchi, Y., Kumagaye, K., Noda, Y., Watanabe, T. X., & Sakakibara, S. (1986) *Biopolymers 25*, S61–S68.
Norton, R. S., Clouse, A. O., Addleman, R., & Allerhand, A. (1977) *J. Am. Chem. Soc. 99*, 79.
Olivera, B. M., McIntosh, J. M., Cruz, L. J., Luque, F. A., & Gray, W. R. (1984) *Biochemistry 23*, 5087–5090.
Ott, K-H., Becker, S., Gordon, R. D., & Rüterjans, H. (1991) *FEBS 278*, 160–166.
Pardi, A., Galdes, A., Florance, J., & Maniconte, D. (1989) *Biochemistry 28*, 5494–5501.
Pardi, A., Billeter, M., & Wüthrich, K. (1984) *J. Mol. Biol. 180*, 741–51.
Ramachandran, G. N., Ramakrishnan, C., & Sasisekharan, V. (1963) *J. Mol. Biol. 7*, 95–99.
Ramilo, C. A., Zafaralla, G. C., Nadasdi, L., Hammerland, L. G., Yoshikami, D., Gray, W. R., Kristipati, R., Ramachandran, J., Miljanich, G., Olivera, B. M., & Cruz, L. J. (1992) *Biochemistry 31*, 9919–9926.
Rance, M., Sørensen, O. W., Bodenhausen, G., Wagner, G., Ernst, R. R., & Wüthrich, K. (1983) *Biochem. Biophys. Res. Comm. 117*, 479.
Richardson, J. S. (1981) *Adv. Protein Chem. 34*, 167–339.
Sibanda, B. L., Blundell, T. L., & Thornton, J. M. (1989) *J. Mol. Biol. 206*, 759–777.
Sklenár, V., Torchia, D., & Bax, A. (1987) *J. Magn. Reson. 73*, 375–79.
Smith, J. L., Corfield, P. W. R., Hendrickson, W. A., & Low, B. W. (1988) *Acta Crystallogr., Sect. A 44*, 357–368.
States, D. J., Haberkorn, R. A., & Ruben, D. J. (1982) *J. Magn. Reson. 48*, 286.
Thomas, P. D., Basus, V. J., & James, T. L. (1991) *Proc. Natl. Acad. Sci. U.S.A. 88*, 1237–41.
Tsien, R. W., Ellinor, P. T., & Horne, W. A. (1991) *Trends Pharm. Sci. 12*, 349.
Valentino, K., Bowersox, S., Smith, M. L., Siesjo, B. K., Singh, T., Gadbois, T., Justice, A., Ramachandran, J., & Hoffman, B. B. (1992) *Soc. Neurosci. Abs. 18*, 1253.
van Gunsteren, W. F., Kaptein, R., & Zuiderweg, E. R. P. (1983) in *Nucleic Acid Conformation and Dynamics* (Olson, W. K., Ed.) pp 79–82, Orsay, France, Report of NATO/CECAM Workshop.
van Gunsteren, W. F., & Berendsen, H. J. C. (1987) *GROMOS manual*, Biomos b. v. Biomolecular Software, Groningen.
Wagner, G., Braun, W., Havel, T. F., Schaumann, T., Gō, N., & Wüthrich, K. (1987) *J. Mol. Biol. 196*, 611–38.
Wilmot, C. M., & Thornton, J. M. (1990) *Protein Eng. 3*, 479–93.
Wüthrich, K. (1986) *NMR of Proteins and Nucleic Acids*, John Wiley & Sons, New York.
Yamashiro, D., & Li, C. H. (1988) *Int. J. Peptide Protein Res. 31*, 322–334.